

Article

Synthesis and Characterization of Amorphous Molybdenum Sulfide (MoS_x)/ CdIn_2S_4 Composite Photocatalyst: Co-Catalyst Using in the Hydrogen Evolution Reaction

Qi Li ¹, Wanli Liu ¹, Xuejian Xie ^{1,2,*}, Xianglong Yang ^{1,2,*}, Xiufang Chen ^{1,2} and Xiangang Xu ^{1,2}

¹ State Key Laboratory of Crystal Materials, Shandong University, Jinan 250100, China; liqi1995@mail.sdu.edu.cn (Q.L.); lwlsdu@mail.sdu.edu.cn (W.L.); cxf@sdu.edu.cn (X.C.); xxu@sdu.edu.cn (X.X.)

² Institute of novel semiconductors, Shandong University, Jinan 250100, China

* Correspondence: xiexj@sdu.edu.cn (X.X.); yangxl2016@sdu.edu.cn (X.Y.); Tel.: +86-183-6611-1581 (X.X.)

Received: 2 December 2020; Accepted: 9 December 2020; Published: 11 December 2020



Abstract: Co-catalyst deposition is used to improve the surface and electrical properties of photocatalysts. In this work, $\text{MoS}_x/\text{CdIn}_2\text{S}_4$ nanocomposites were prepared by a facile hydrothermal and photodeposition route. The basic crystalline phases and morphology of the as-prepared samples were determined, and these results showed that MoS_x was tightly anchored onto CdIn_2S_4 by sharing the same S atom. In the hydrogen production experiments, $\text{MoS}_x/\text{CdIn}_2\text{S}_4$ -40 displayed the optimal photocatalytic hydrogen production yield in 4 h. The H_2 evolution rate reached 2846.73 $\mu\text{mol/g/h}$, which was 13.6-times higher than that of pure CdIn_2S_4 . Analyzing the photocatalytic enhancement mechanisms revealed that this unique structure had a remarkable photogenerated electron-hole pair separation efficiency, rapid charge carrier transfer channels, and more abundant surface reaction sites. The use of co-catalyst (MoS_x) greatly improved the photocatalytic activity of CdIn_2S_4 .

Keywords: co-catalyst; photocatalyst; hydrogen production; CdIn_2S_4 ; MoS_x

1. Introduction

Hydrogen is a renewable energy source that can possibly solve the energy crisis and environmental pollution, but its conversion method must be further explored to enable its practical application. Various scholars have studied methods to efficiently produce hydrogen [1,2]. Photocatalysis is a low-cost and convenient method to convert solar energy into hydrogen energy [3]. This energy transformation method requires a photocatalyst that can absorb solar energy to drive the hydrogen evolution reaction. Numerous studies have reported developing photocatalysts such as metal oxides [4], nitrides [5], sulfides [6], and metal-free semiconductors [7]. Unfortunately, it is difficult for these semiconductors to achieve efficient hydrogen production in practical applications because of their poor visible light absorption, which leads to low hydrogen production [8].

Various photocatalysts have been explored to absorb more visible light for photocatalytic hydrogen production. Among them, typical layered transition metal chalcogenides (TMCs) have garnered much attention due to their high-performance hydrogen production capacities and tunable band gaps [9]. Cadmium indium sulfide (CdIn_2S_4) is a TMC with excellent visible light-harvesting capacity due to its suitable and tunable band gap [10]. Its regular shape and convenient preparation method have caused it to receive significant attention as a hydrogen production photocatalyst. For example, Li described the controllable synthesis of CdIn_2S_4 , whose band gap (2.06–2.85 eV) could be regulated by adjusting the Cd/In ratio to allow CdIn_2S_4 to harvest more visible light [11]. As a result, CdIn_2S_4 showed

remarkable photocatalytic activity compared with CdS; however, the photocatalyst only showed good photocatalytic hydrogen production efficiency when it was attached to a noble metal [12]. This work indirectly verified that pure CdIn₂S₄ cannot satisfy the requirements of practical applications, despite the above advantages. In another study, its lower photocatalytic hydrogen production efficiency was attributed to the recombination of photogenerated carriers and a low surface area for the hydrogen evolution reaction [13]; therefore, it is important to further enhance the photocatalytic performance of pure CdIn₂S₄.

Many efforts have been made to improve the hydrogen production capability using co-catalyst deposition [14], doping [15], morphology designing [16,17], and heterojunction construction [18]. Among these, co-catalyst deposition is well-known for its ability to modify photocatalysts, and a good photocatalytic co-catalyst must exhibit effective electron transport channels and a promising capacity for the hydrogen evolution reaction [14]. Co-catalysts such as Pt have been used to improve the photocatalytic capacity because Pt offers a promising reaction surface for hydrogen production as well as a remarkable electron transfer rate during photogenerated electron transport. It has been widely used in contact photocatalysts such as TiO₂, C₃N₄, and CdS [19]; however, noble metals cannot be used for large-scale applications because they are expensive. Thus, it is essential to rationally combine co-catalysts for higher hydrogen production efficiencies.

This problem can be solved by using amorphous molybdenum sulfides (MoS_x), which have been shown to greatly activate and stabilize the hydrogen evolution reaction (HER), especially in acidic solutions. They are also expected to become substitutes for noble metals [20]. Compared with MoS₂, MoS_x can also be synthesized in a milder environment. Though the S atoms in amorphous molybdenum sulfides show long-range disorder, short-range atomic arrangements offer more surface area for the hydrogen evolution reaction. Due to this, the deposition of amorphous molybdenum sulfides has proven to be a promising way to improve photocatalytic hydrogen production. MoS_x not only offers electron transport channels that promote the separation of electron-hole pairs, but also act as active reaction sites [21–23]. MoS_x is a noble-metal-free material whose hydrogen evolution activity is better than that of MoS₂. Moreover, MoS_x/CdS composite photocatalysts were synthesized by assembling MoS_x onto CdS nanorods for hydrogen production. MoS_x shared an S atom with CdS during deposition, which helped build rapid electron transport channels between CdS and MoS_x, leading to a remarkable hydrogen production yield [22]. According to the survey above, this paper aimed to synthesize MoS_x/CdIn₂S₄ composite photocatalysts with improved hydrogen production.

In this study, pure CdIn₂S₄ was prepared by a one-step hydrothermal method, and MoS_x was then deposited onto the surface of CdIn₂S₄ via a photodeposition method for the HER (Figure 1). The crystalline phase and morphologies of MoS_x/CdIn₂S₄ composites were systematically studied to verify how MoS_x deposition affected the morphology and crystalline phases. The MoS_x/CdIn₂S₄ photocatalyst showed remarkable photocatalytic activity, and the optimal deposition ratio of MoS_x for the HER was investigated. MoS_x/CdIn₂S₄-40 showed the best hydrogen production yield, which was 13.6 times higher than that of CdIn₂S₄, and its H₂ evolution rate reached 2846.73 μmol/g/h. The optical and electrochemical characteristics of MoS_x/CdIn₂S₄ composites were measured to explore the improvement mechanism. In the photocatalyst system, MoS_x provided sites for hydrogen production and acted as a charge acceptor to separate photogenerated electron-hole pairs. In all, considering the convenient and mild preparation conditions of MoS_x/CdIn₂S₄, MoS_x helped improve the photocatalytic capacity of CdIn₂S₄ and offers an attractive method to enhance the photocatalytic hydrogen evolution using CdIn₂S₄.

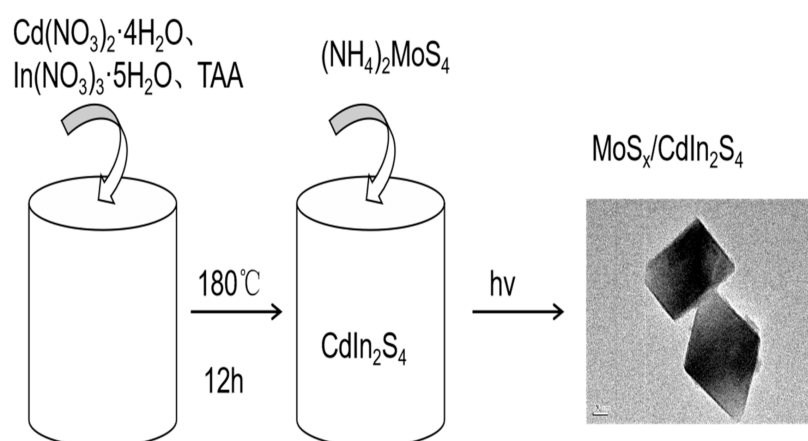


Figure 1. The synthesis method of $\text{MoS}_x/\text{CdIn}_2\text{S}_4$. $\text{MoS}_x/\text{CdIn}_2\text{S}_4$ composites were prepared by a photodeposition method and products were prepared by changing the exposure time and were named by different exposure time: $\text{MoS}_x/\text{CdIn}_2\text{S}_4$ -20, $\text{MoS}_x/\text{CdIn}_2\text{S}_4$ -40, and $\text{MoS}_x/\text{CdIn}_2\text{S}_4$ -60.

2. Results

2.1. Crystalline Structure

First, X-Ray Diffraction (XRD) patterns were collected to verify the chemical components of test samples (Figure 2). All samples displayed similar XRD patterns, with main peaks at 14.14° , 23.18° , 27.25° , 28.48° , 33.00° , 40.74° , 43.32° , and 47.41° for crystalline CdIn_2S_4 . These peaks were fitted to the (111), (220), (311), (222), (400), (442), (511), and (440) planes of cubic CdIn_2S_4 (PDF#27-0060) [11]. The above results indicated that all samples contained cubic CdIn_2S_4 , and that the main photocatalyst CdIn_2S_4 remained unchanged during synthesis; however, no XRD peak for MoS_x was observed in the $\text{MoS}_x/\text{CdIn}_2\text{S}_4$ samples, mainly because of the amorphous structure of MoS_x [22]. Therefore, it is necessary to use a different method to detect the presence of MoS_x .

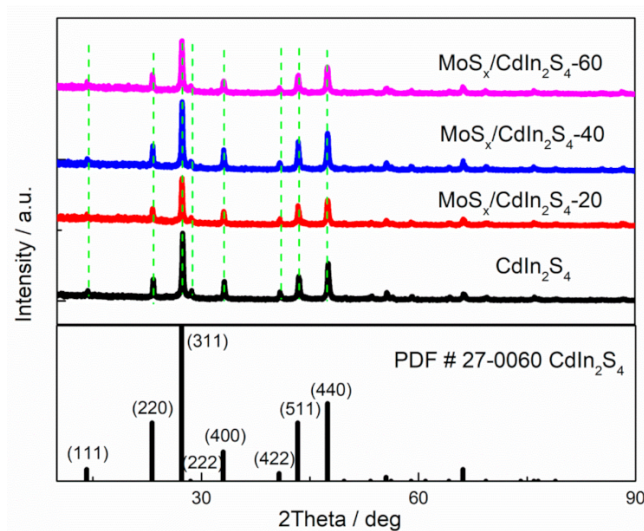


Figure 2. X-Ray Diffraction (XRD) patterns of the as-prepared samples.

X-ray photoelectron spectroscopy (XPS) spectra were collected to investigate the surface chemical composition and states of the as-prepared samples. The survey spectra of Cd, In, and S of pure CdIn_2S_4 and $\text{MoS}_x/\text{CdIn}_2\text{S}_4$ -40 are shown in Figure 3. The Mo spectrum was not detected in the survey spectra of $\text{MoS}_x/\text{CdIn}_2\text{S}_4$ due to the low Mo content. The high-resolution S 2p spectra of CdIn_2S_4 can be deconvoluted into two peaks at 161.30 eV and 162.50 eV, which were assigned to the $2p_{3/2}$ and $2p_{1/2}$

chemical states levels of S^{2-} [11]. After deposition with MoS_x , the S 2p spectrum can be divided into three peaks, and the extra weak peak at 163.26 eV was identified as unsaturated S, which is its typical chemical state in MoS_x [22,23]. Previous reports also support the observation that MoS_x contains special unsaturated active S, further indicating the presence of MoS_x on the surface. Compared with bare $CdIn_2S_4$, $MoS_x/CdIn_2S_4$ displays weak Mo 3d peaks at 228.04 eV, 229.40 eV, 229.74 eV, 232.10 eV, and 232.61 eV. The peaks at 228.04 eV, 229.40 eV, and 229.74 eV belonged to Mo 3d5, Mo 3d, and Mo S2 due to Mo^{4+} in MoS_2 or MoS_3 [20,23,24]. The doublet peaks at 232.1 and 232.61 eV were assigned to Mo^{6+} in MoS_3 . The slight increase in peak value of the high-resolution Cd 3d and In 3d spectra was mainly caused by interactions between MoS_x and $CdIn_2S_4$. These results revealed that MoS_x existed on the surface of $CdIn_2S_4$. Combined, the XPS and XRD results showed that the as-prepared sample was mainly composed of MoS_x and $CdIn_2S_4$.

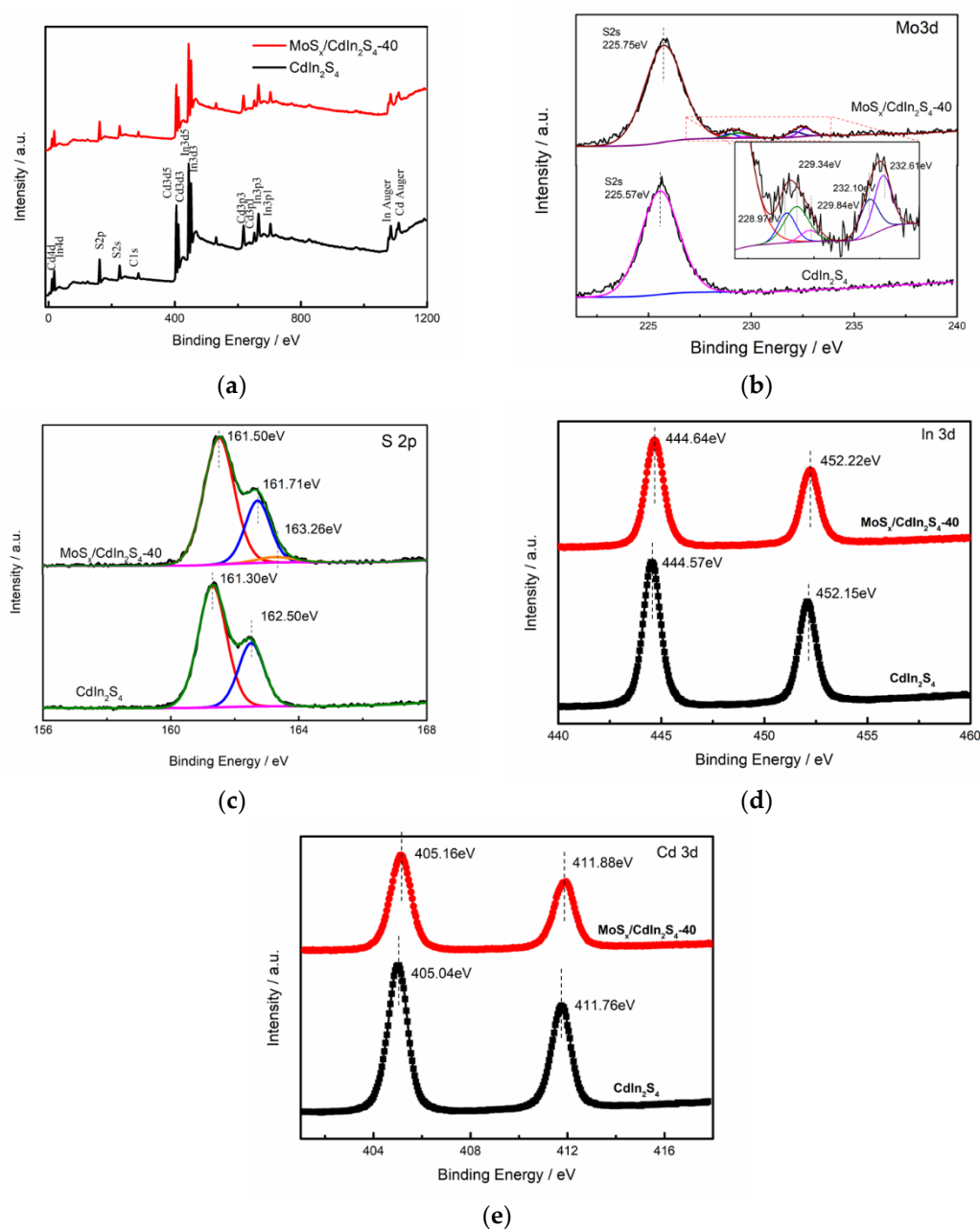


Figure 3. X-ray photoelectron spectroscopy (XPS) spectra of $CdIn_2S_4$ and $MoS_x/CdIn_2S_4$. Survey spectra (a); high-resolution spectra of Cd (b); In (c); Mo (d); and S (e).

2.2. Morphology

Scanning electron microscope (SEM) was used to characterize the morphology of all samples, and EDS was used to determine the corresponding dispersion of elements. As displayed in Figure 4, pure CdIn_2S_4 showed many symmetrical nanoflake microspheres that were 50–70 nm long, which were stacked into large nanoparticles. These small symmetrical nanoflake microspheres provided a large surface area for solar energy harvesting and hydrogen evolution reaction, which led to remarkable photocatalytic efficiency. However, nothing obvious changed in the $\text{MoS}_x/\text{CdIn}_2\text{S}_4$ composite after photodeposition, mainly because of the low concentration of MoS_x . This result does not indicate that MoS_x was deposited onto the surface of CdIn_2S_4 in situ, but it does confirm that CdIn_2S_4 remained unchanged during photodeposition.

To further determine the corresponding concentrations of elements, Energy Dispersive Spectroscopy (EDS) was carried out. The EDS (Figure 5) results of $\text{MoS}_x/\text{CdIn}_2\text{S}_4$ showed a low Mo content in the composite, which indirectly indicates that MoS_x was present in 0.83% (the content of MoS_x also shown in Table S2). The elemental mapping image shows that Mo was uniformly dispersed on the composite surface, which confirmed that MoS_x was very evenly distributed in the composite.

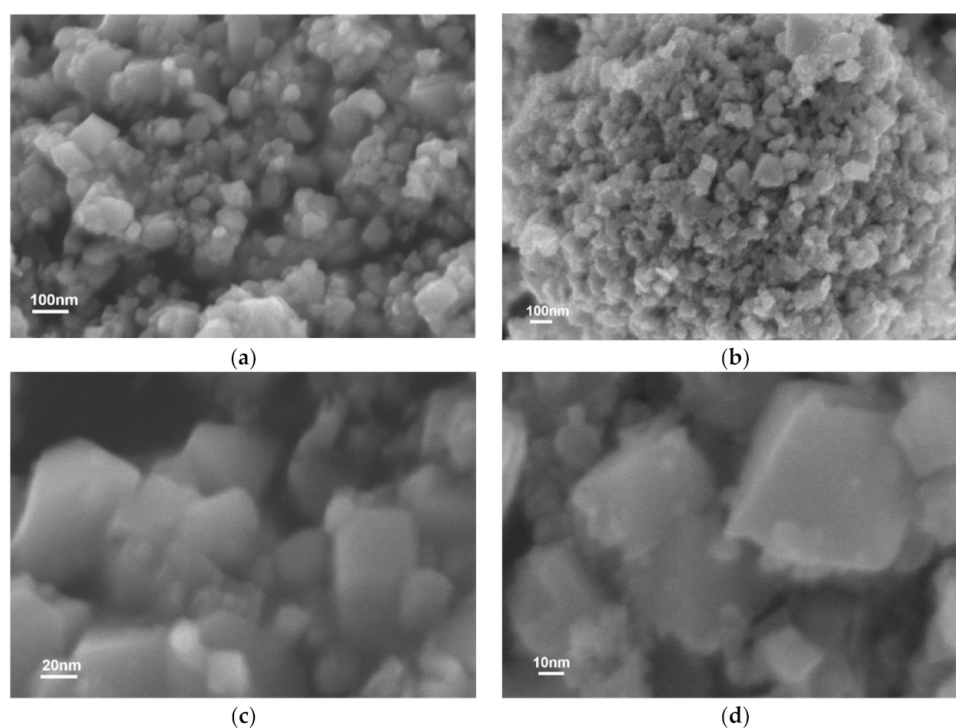


Figure 4. SEM image of CdIn_2S_4 (a,c) and $\text{MoS}_x/\text{CdIn}_2\text{S}_4$ (b,d).

Transmission electron microscope (TEM) and high resolution transmission electron microscopy (HRTEM) were used to confirm the crystallinity and morphology of samples in Figure 6. The images showed the morphology of bare CdIn_2S_4 , which contained thin nanoflakes with a few curved nanoflakes. Each nanoflake in the SEM image was about 40–80 nm wide. The crystal lattice spacing of CdIn_2S_4 determined by HRTEM was 0.329 nm, 0.385 nm, and 0.629 nm, which can be indexed to the (311), (220), and (111) planes of cubic spinel CdIn_2S_4 from the comparison with XRD patterns. The TEM images after deposition showed that the surface of CdIn_2S_4 was covered with irregular MoS_x nanoparticles with edge lengths of 9.159 nm. The HRTEM image showed that highly disordered crystals were attached to the nanoflakes, which showed similar single-crystal lattices. This confirmed that MoS_x was closely attached to the CdIn_2S_4 surface via a common S atom, which helped construct rapid electron transport channels that may improve the photocatalytic capacity.

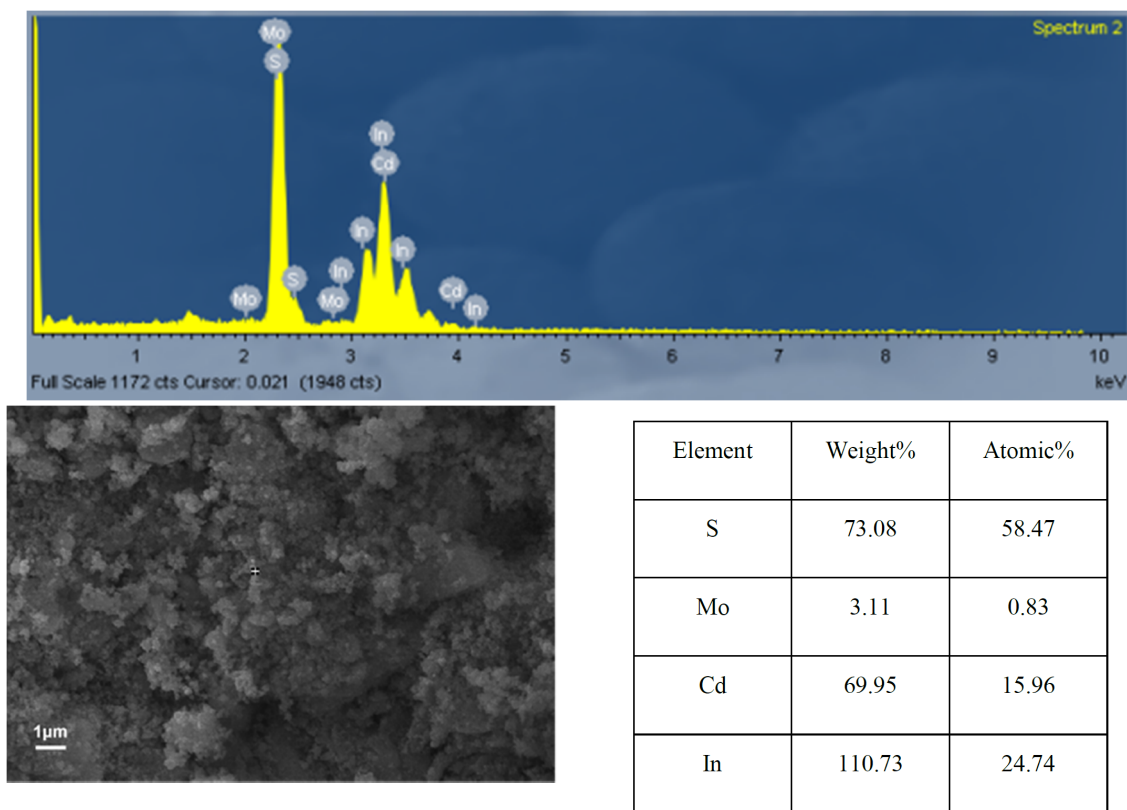


Figure 5. EDS results of Mo_x/CdIn₂S₄.

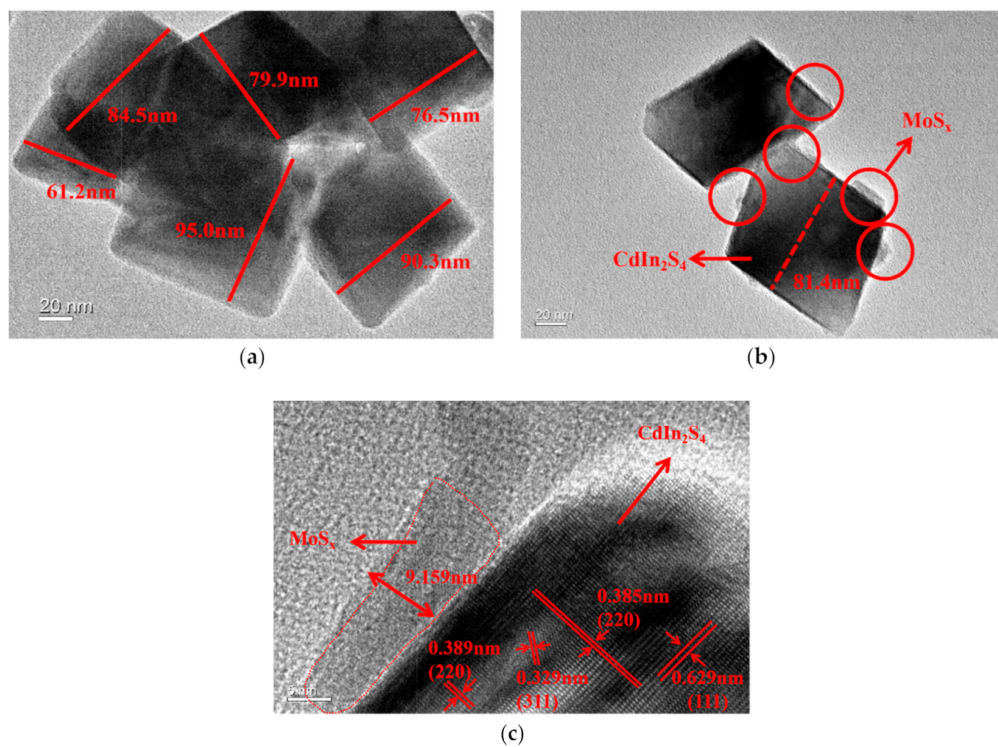


Figure 6. Transmission electron microscope (TEM) image of CdIn₂S₄ (a) and Mo_x/CdIn₂S₄ (b,c).

2.3. Photocatalytic Activity

Hydrogen evolution experiments were carried out under visible light irradiation to measure the photocatalytic capacity of the as-prepared samples. The sacrificial reagent (0.1 M Na₂SO₃/Na₂S solution) was used to react with photogenerated holes. As shown in Figure 7, the same condition without sunlight and the same condition with blank samples were performed to determine the effects of disturbed elements. The photocatalytic production yields of pure samples of CdIn₂S₄, Pt/CdIn₂S₄ (XRD was shown in Figure S1), MoS₂/CdIn₂S₄, and MoS_x/CdIn₂S₄ were also presented. Pure CdIn₂S₄ showed minimal H₂ evolution yield under visible light irradiation, and the average rate reached 209.41 μmol/g/h in 4 h. After co-catalyst deposition, the hydrogen evolution of MoS₂/CdIn₂S₄ and Pt/CdIn₂S₄ reached 1265.12 μmol/g/h and 1451.71 μmol/g/h, respectively. This result was attributed to the fact that co-catalyst deposition increased the number of active sites, and many electron transport channels emerged [25]. In this work, the hydrogen production yields of MoS_x/CdIn₂S₄-20, MoS_x/CdIn₂S₄-40, and MoS_x/CdIn₂S₄-60 were greatly enhanced due to the presence of the MoS_x co-catalyst. MoS_x/CdIn₂S₄-40 displayed the greatest H₂ evolution rate of 2846.73 μmol/g/h, which indicates that MoS_x/CdIn₂S₄ was the best photocatalyst. Its hydrogen evolution rate was about 13.6 and 2.25 times higher than pure CdIn₂S₄ and MoS₂/CdIn₂S₄. In addition, the MoS_x content also affected the photocatalytic hydrogen production, and the hydrogen evolution rates first increased upon increasing the deposited amount of MoS_x and then decreased. This revealed that the optimal amount of MoS_x on CdIn₂S₄ affected the photocatalytic hydrogen production capacity of the composites. All hydrogen evolution experimental results showed that MoS_x/CdIn₂S₄ is a promising photocatalyst for hydrogen production.

Photocatalyst stability is also important for practical applications; therefore, the cycling runs of hydrogen production were carried out to determine the photocatalyst stability. The picture displays the hydrogen production amounts of the as-prepared composites for different numbers of 4-h photocatalytic hydrogen production cycles. The hydrogen production amount only slightly decreased after each cycle, showing that the photocatalytic capacity of MoS_x/CdIn₂S₄-40 remained nearly constant. The photocatalyst crystal structure stability can be further characterized by comparing the pattern of MoS_x/CdIn₂S₄-40 before hydrogen evolution and after three cycles. The crystal structure of the photocatalyst exhibited similar XRD patterns before and after the cycle experiments, suggesting that MoS_x/CdIn₂S₄-40 is a sufficiently stable photocatalyst for practical applications.

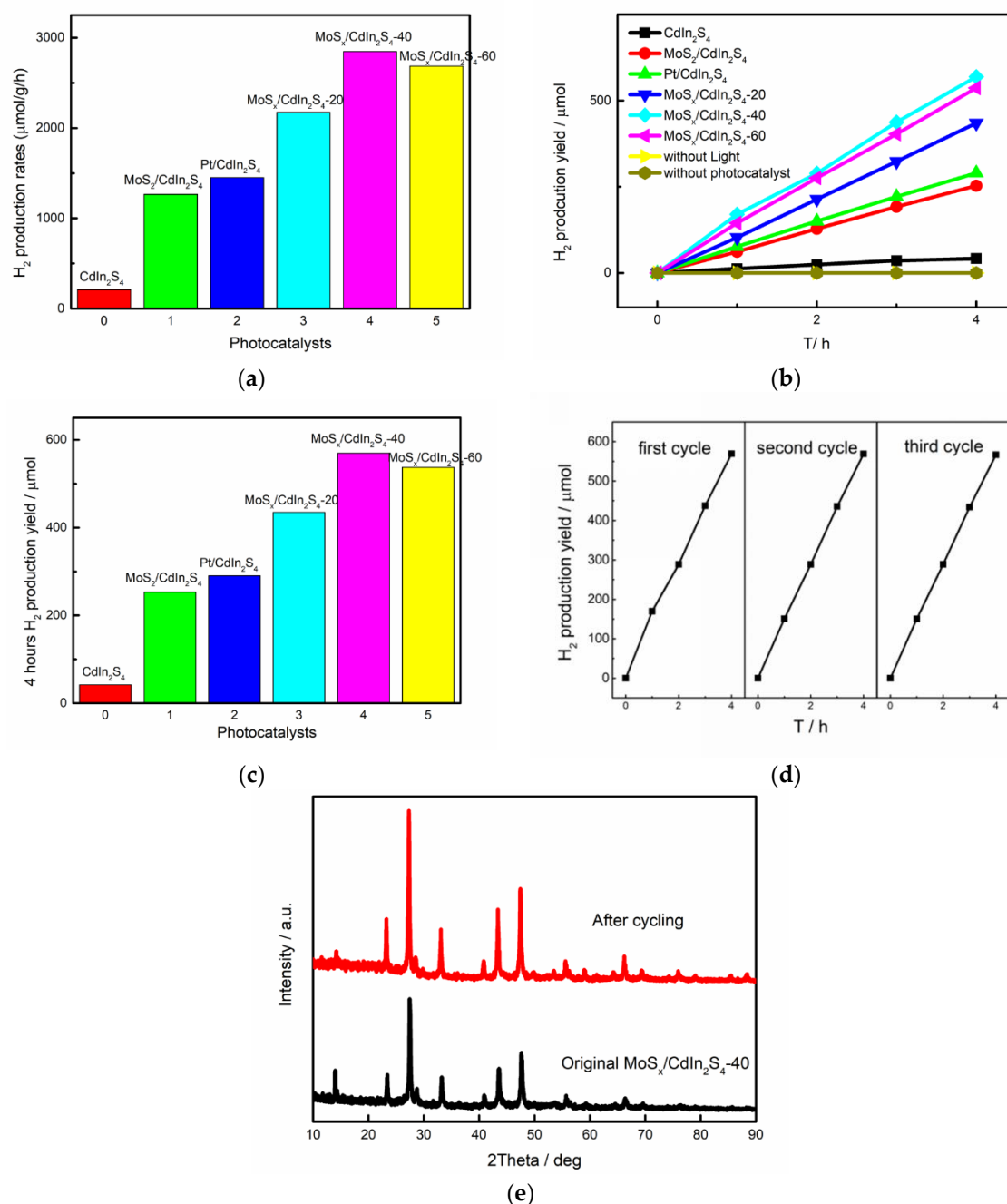


Figure 7. (a) H₂ production yield, (b) H₂ production yield over 4 h, (c) H₂ production rates of the as-prepared samples, (d) photocatalytic cycle tests of MoS_x/CdIn₂S₄-40 composites, and (e) XRD patterns of the MoS_x/CdIn₂S₄-40 composite after photocatalytic cycles.

2.4. Photocatalytic Mechanism

The photocatalytic hydrogen production yield closely depends on the generation, transport, and reactions of photogenerated charge carriers. The generation of electron-hole pairs is determined by a material's bandgap, and a bandgap that matches harvested visible light is required. Ultraviolet-visible (UV-Vis) spectra, XPS valence band spectra, and Mott-Schottky spectra were obtained to explore the bandgaps of the as-prepared samples. As illustrated in Figure 8a, pure CdIn₂S₄ showed a fundamental absorption edge at 470 nm, which revealed that pure CdIn₂S₄ has broad light absorption in the visible light region. However, the absorption edge of the MoS_x/CdIn₂S₄ composites was located at 500 nm, and this blue-shift means that the photocatalyst had improved visible light absorption, which should

sharply increase the photogenerated charge carriers. This result was attributed to the fact that MoS_x shared S atom with CdIn_2S_4 during photodeposition, which changed a small portion of the crystalline phase on the surface, leading to a blue-shift of the absorption edge. Similar to the literature, the bandgap of the as-prepared composite can be calculated by the formula: $\alpha h\nu = C(h\nu - E_g)^2$. The band gap of pure CdIn_2S_4 was 2.18 eV, which is similar to a previous report [25]. However, the bandgap of $\text{MoS}_x/\text{CdIn}_2\text{S}_4$ was 2.04 eV, which was attributed to the addition of MoS_x , which improved the visible light harvesting. To further explore the photocatalytic band structures, XPS valence band spectroscopy and impedance-potential tests were carried out. XPS valence band spectra were used to directly determine the valence band (VB) of the as-prepared samples and their flat-band (FB) potentials, which were roughly equivalent to the conduction band (CB). These were calculated by the Mott–Schottky plot of the impedance–potential test. The E_{FB} of CdIn_2S_4 and $\text{MoS}_x/\text{CdIn}_2\text{S}_4$ were -0.489 and -0.454 V vs. NHE, and E_{FB} of the sample, according to the ordinate of the fitted straight line in the Mott–Schottky plot. According to the formula: $E_{\text{CB}} = E_{\text{VB}} - E_g$ and $E_{\text{CB}} \approx E_{\text{FB}}$, the E_{VB} was calculated using E_{CB} . The general band structures (shown in the plot) were determined from the UV–Vis spectra and E_{FB} . $\text{MoS}_x/\text{CdIn}_2\text{S}_4$ had the optimal band structure of all materials, which should boost the hydrogen production yield.

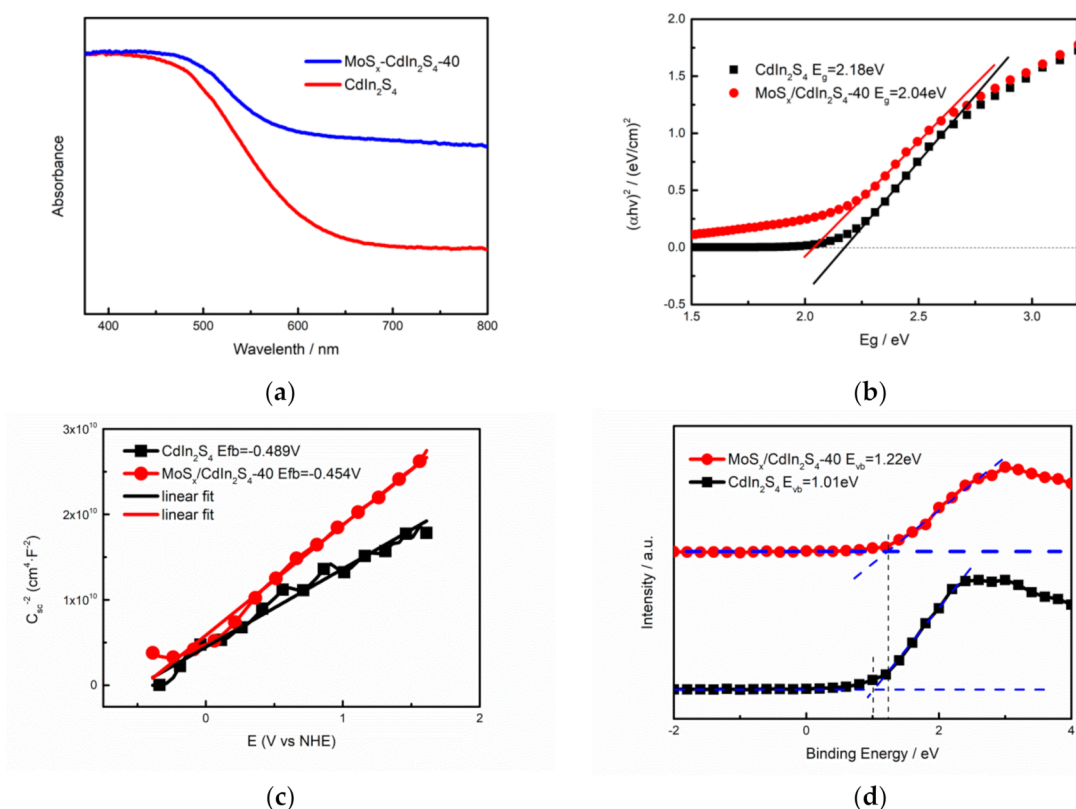


Figure 8. UV–Vis spectra (a), Tauc plots (b), Mott–Schottky plots (c), and XPS valence band spectra of CdIn_2S_4 and $\text{MoS}_x/\text{CdIn}_2\text{S}_4$ (d).

Photoelectrochemical characterization techniques were used to further investigate the interfacial photogenerated charge separation and transfer in the as-prepared samples. The transient photocurrent responses of CdIn_2S_4 , $\text{MoS}_x/\text{CdIn}_2\text{S}_4$ -20, $\text{MoS}_x/\text{CdIn}_2\text{S}_4$ -40, and $\text{MoS}_x/\text{CdIn}_2\text{S}_4$ -60 were tested. As shown in Figure 9a, the photocurrent rapidly reached a maximum when the light was switched on, indicating that photogenerated electron-hole pairs were produced by visible light. The significant differences in photocurrent density depended on the photogenerated charge separation and transfer. The pure CdIn_2S_4 photocatalyst showed a low photocurrent density, which means that photogenerated charge separation and transfer represented a considerable loss in energy. Similar to a previous

report [26], pure CdIn_2S_4 consumed significant amounts of energy because of the rapid recombination of photogenerated electron-hole pairs. The introduction of MoS_x solved this problem, and the photocurrents of $\text{MoS}_x/\text{CdIn}_2\text{S}_4$ -20, $\text{MoS}_x/\text{CdIn}_2\text{S}_4$ -40, and $\text{MoS}_x/\text{CdIn}_2\text{S}_4$ -60 sharply increased to 2.71, 4.56, and 1.91 μA , respectively. The photocurrent of $\text{MoS}_x/\text{CdIn}_2\text{S}_4$ -40 was 7.5 times higher than that of CdIn_2S_4 . Noticeably, corresponding to the hydrogen production yields, $\text{MoS}_x/\text{CdIn}_2\text{S}_4$ -40 showed the highest photocurrent intensity. The transient photocurrent responses of the as-prepared samples confirmed that MoS_x improved the charge separation and transfer capacity in CdIn_2S_4 , which should lead to remarkable hydrogen production.

Electrochemical Impedance Spectroscopy (EIS) was used to measure the charge transfer efficiency. Nyquist plots can be obtained by EIS, and the Nyquist plots of the as-prepared samples were explained by a circuit model. This circuit model includes ohmic series resistance (R_1), electron transfer resistance (R_2), a constant-phase element (C_1), and Warburg resistance (W). The electron transfer resistance (R_2) corresponds to the diameter of the semicircular arc, in which a smaller diameter indicates a smaller resistance, which leads to the rapid transfer of photogenerated charge carriers [25]. The diameter of the semicircular arc of $\text{MoS}_x/\text{CdIn}_2\text{S}_4$ -40 was smaller than that of CdIn_2S_4 , revealing that the mobility of photogenerated charges was higher in $\text{MoS}_x/\text{CdIn}_2\text{S}_4$ -40.

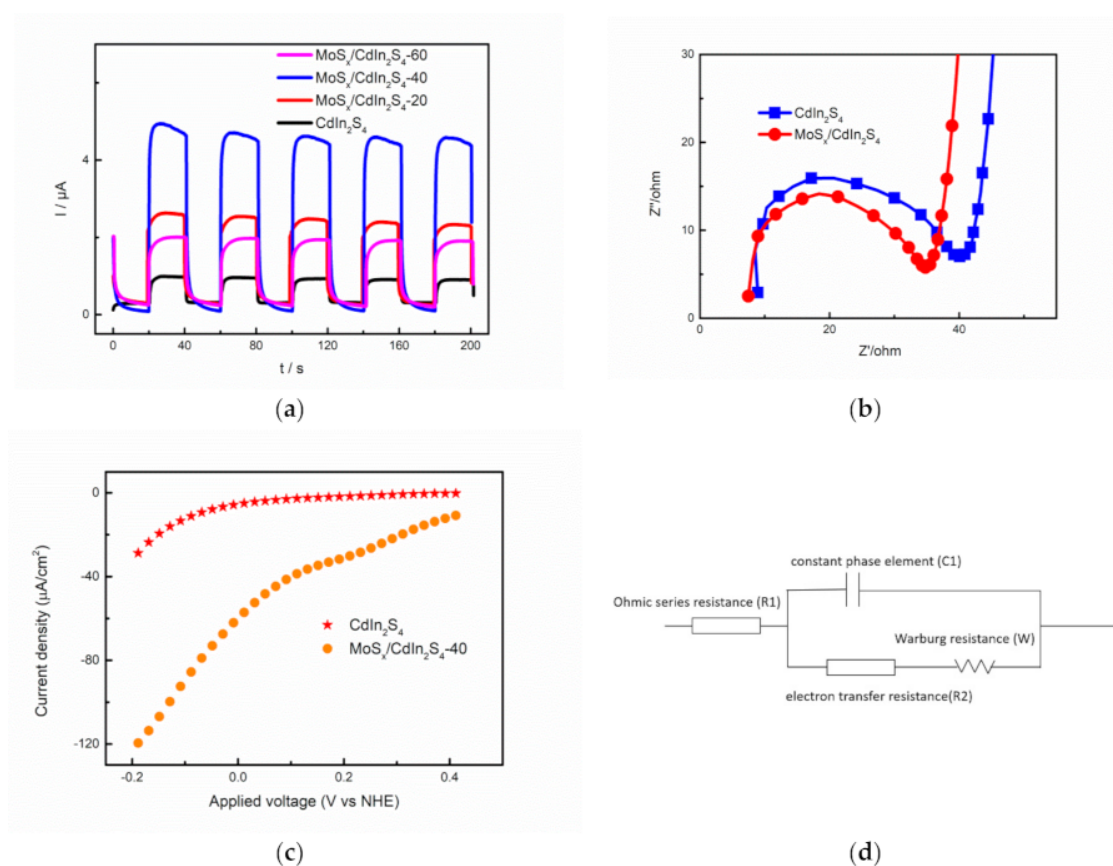


Figure 9. Transient photocurrent responses (a) of CdIn_2S_4 and $\text{MoS}_x/\text{CdIn}_2\text{S}_4$; Electrochemical Impedance Spectroscopy (EIS) Nyquist (b) and Linear sweep voltammograms (LSV) (c) plots of CdIn_2S_4 and $\text{MoS}_x/\text{CdIn}_2\text{S}_4$; the circuit model (d) in the EIS Nyquist plot.

Photogenerated charges were separated and transferred to the surface reaction sites to participate in the hydrogen evolution reaction. Linear sweep voltammograms (LSV) of the as-prepared samples were obtained to determine the surface hydrogen production reactions of CdIn_2S_4 and $\text{MoS}_x/\text{CdIn}_2\text{S}_4$ -40. In the LSV polarization curves of the as-prepared samples, $\text{MoS}_x/\text{CdIn}_2\text{S}_4$ displayed a larger slope and current compared with bare CdIn_2S_4 , which means that $\text{MoS}_x/\text{CdIn}_2\text{S}_4$ -40 more easily produced

hydrogen at the same photovoltage. This reveals that faster hydrogen production would occur using MoS_x/CdIn₂S₄-40 at the same voltage. These results reveal that MoS_x/CdIn₂S₄-40 has superior reaction sites for hydrogen production.

The combined results showed that the MoS_x/CdIn₂S₄-40 photocatalyst showed remarkable photocatalytic hydrogen evolution because of its unique structure. Pure CdIn₂S₄ photocatalyst shares the same S atom with MoS_x, which provided the perfect anchor point for MoS_x, leading to tight bonding between CdIn₂S₄ with MoS_x. This unique linking improved the light-harvesting of the pure CdIn₂S₄ photocatalyst and increased the separation and transfer of photogenerated charges. MoS_x is an efficient co-catalyst with abundant hydrogen evolution sites. Furthermore, MoS_x and CdIn₂S₄ formed a classical Schottky structure with tight linking, and this structure further improved the charge carrier separation and electron transfer. This increased the number of reacting electrons, which ultimately led to its remarkable photocatalytic hydrogen production rate.

3. Experimental

3.1. Chemical Reagents

All chemical reagents were analytical reagent grade, and they were used as received without further purification. Indium nitrate hydrate (In(NO₃)₃·5H₂O), cadmium nitrate tetrahydrate (Cd(NO₃)₂·4H₂O), sodium sulfide nonahydrate (Na₂S·9H₂O), sodium sulfite (Na₂SO₃), sodium sulfate (Na₂SO₄), thioacetamide (TAA), and ethanol were obtained from Aladdin (Shanghai, China).

3.2. Synthesis of MoS_x/CdIn₂S₄ Composites

The synthesis process of MoS_x/CdIn₂S₄ composites is shown in Figure 1.

Pure CdIn₂S₄ was prepared by a simple hydrothermal method according to the literature [10]. Briefly, 0.1232 g of Cd(NO₃)₂·4H₂O, 0.3056 g of In(NO₃)₃·5H₂O, and 0.2404 g of TAA were successively added in 15 mL deionized water. After that, this mixture was vigorously stirred for 0.5 h. The solution was then placed into a 50 mL Teflon-lined autoclave and kept at 180 °C for 12 h. Afterward, yellow samples, which were pure CdIn₂S₄, were obtained by filtration and washed with deionized water and ethanol. The desired product was dried at 60 °C.

MoS_x/CdIn₂S₄ composites were prepared by a photodeposition method according to the literature [22]. In this experiment, 100 mg pure CdIn₂S₄ nanoparticles were added to a mixed solvent (water:ethanol = 4:1) with stirring. After 20 min stirring, 8.5 mg (NH₄)₂MoS₄ (synthesized using a previously reported method [22]) were dissolved into the mixed solution. Then, this suspension was stirred for 30 min to reach the adsorption–desorption equilibrium. The as-prepared mixture was poured into a photocatalytic reactor. During photodeposition, a 300 W Xenon lamp was used to simulate solar irradiation, and the mixture was held at 6 °C with continuous stirring for 40 min. After photodeposition, a greenish-yellow product was obtained after centrifugation and washing. The product was dried at 60 °C, and the as-prepared sample was named MoS_x/CdIn₂S₄-40. Similar products were prepared by changing the exposure time and were named MoS_x/CdIn₂S₄-20 and MoS_x/CdIn₂S₄-60. MoS₂/CdIn₂S₄ and Pt/CdIn₂S₄ were prepared by the method similar to the report [17].

3.3. Characterization

X-ray diffraction (XRD) patterns of synthesized catalysts were obtained on a D8-advance x-ray diffractometer (Bruker, Billerica, MA, USA) using Cu Kα (λ = 0.15406 nm) radiation. The UV–Vis diffuse reflectance spectra (DRS) were obtained on a UV-2550 UV–Vis spectrophotometer (Shimadzu, Tokyo, Japan), which used BaSO₄ as a reflectance standard. The scanning electron microscope (SEM) images and energy-dispersive x-ray spectra (EDS) were recorded by a HITACHI S-4800 field emission SEM. Transmission electron microscope (TEM) and high-resolution TEM (HRTEM) images were obtained using a high-resolution TEM (JEOL, JSM-2100F, Tokyo, Japan).

3.4. Hydrogen Production and Electrochemical Experiments

The photocatalytic performance was characterized by hydrogen production experiments, in which 50 mg of the as-prepared photocatalysts was dispersed in 50 mL aqueous solution with string. Then, 0.1 M aqueous $\text{Na}_2\text{S}/\text{Na}_2\text{SO}_3$ was used as the sacrificial agent. After that, the solution was dropped into a photocatalytic reactor that was irradiated by a 300 W Xenon lamp to simulate visible light irradiation. The entire photocatalytic reaction system was held at 7 °C to produce hydrogen. The final obtained generated hydrogen yields were detected by gas chromatography (GC-7900, TCD, Ar carrier).

An electrochemical workstation was used to measure the electrochemical characteristics of the photocatalysts. In these experiments, samples were prepared by coating them onto indium tin oxide (ITO) glass. This test system was a three-electrode cell, with ITO as the working electrode, Ag/AgCl as the reference electrode, and a 1 cm × 1 cm platinum film as the counter electrode. Similar to the hydrogen production experiment, a 300 W Xenon lamp was used to simulate solar light. The photocurrent was recorded at a bias voltage of 0.2 V (vs. Ag/AgCl) with light irradiation. The electrochemical impedance spectra (EIS) were obtained in the frequency range from 1 to 106 Hz. The flat-band voltage was measured at bias voltages between 1 V to −1 V (vs. Ag/AgCl).

4. Conclusions

The composite photocatalyst $\text{MoS}_x/\text{CdIn}_2\text{S}_4$ was synthesized by a facile photodeposition method. XRD, XPS, SEM, EDS, and TEM were used to determine the chemical phase characteristics of the as-prepared catalysts. The results verified the intimate contact between MoS_x and CdIn_2S_4 . The as-prepared $\text{MoS}_x/\text{CdIn}_2\text{S}_4$ -40 composite showed a remarkable hydrogen production rate that was 13.6 times higher than that of pure CdIn_2S_4 . From the optical and photoelectrochemical techniques, this was attributed to intimate interfacial contact, which produced abundant reaction sites, better charge separation, and better electron transfer efficiency. MoS_x offers many hydrogen evolution sites for hydrogen production. In addition, $\text{MoS}_x/\text{CdIn}_2\text{S}_4$ -40 exhibited outstanding stability (Table S1), which will advance its practical applications, and this study offers guidance for photocatalytic hydrogen production.

Supplementary Materials: The following are available online at <http://www.mdpi.com/2073-4344/10/12/1455/s1>, Figure S1: XRD of $\text{Pt}/\text{CdIn}_2\text{S}_4$ and $\text{MoS}_2/\text{CdIn}_2\text{S}_4$, Table S1: The quantum yields of different material. Table S2: The binding energy (BE) of different element atomic.

Author Contributions: Conceptualization, Q.L.; Methodology, Q.L. and W.L.; Software, Q.L.; Validation, Q.L.; Formal analysis, Q.L.; Investigation, Q.L. and W.L.; Resources, Q.L. and X.Y.; Data curation, Q.L.; Writing—original draft preparation, Q.L.; Writing—review and editing; X.X. (Xuejian Xie) and X.C.; Visualization, X.X. (Xuejian Xie); Supervision, X.X. (Xuejian Xie) and X.Y.; Project administration, X.X. (Xiangang Xu) and X.Y.; Funding acquisition, X.X. (Xuejian Xie) and X.Y. All authors have read and agreed to the published version of the manuscript.

Funding: This work was supported by the National Key R&D Program of China (Grant No. 2018 YFB0905701), the Youth Program of the National Natural Science Foundation of China (Grant No. 51902182), the Outstanding Youth Fund of Shandong Province (Grant No. ZR2019 JQ01), and the Natural Science Foundation of Shandong Province (Grant No. ZR2019 BEM011).

Conflicts of Interest: The authors declare no conflict of interest.

References

1. Wang, Z.; Li, C.; Domen, K. Recent developments in heterogeneous photocatalysts for solar-driven overall water splitting. *Chem. Soc. Rev.* **2019**, *48*, 2109–2125. [[CrossRef](#)] [[PubMed](#)]
2. Lin, L.; Yu, Z.; Wang, X. Crystalline Carbon Nitride Semiconductors for Photocatalytic Water Splitting. *Angew. Chem. Int. Ed.* **2019**, *58*, 6164–6175. [[CrossRef](#)] [[PubMed](#)]
3. Wang, Y.; Suzuki, H.; Xie, J.; Tomita, O.; Martin, D.J.; Higashi, M.; Kong, D.; Abe, R.; Tang, J. Mimicking Natural Photosynthesis: Solar to Renewable H₂ Fuel Synthesis by Z-Scheme Water Splitting Systems. *Chem. Rev.* **2018**, *118*, 5201–5241. [[CrossRef](#)] [[PubMed](#)]

4. Lee, K.; Yoon, H.; Ahn, C.; Park, J.; Jeon, S. Strategies to improve the photocatalytic activity of TiO₂: 3D nanostructuring and heterostructuring with graphitic carbon nanomaterials. *Nanoscale* **2019**, *11*, 7025–7040. [[CrossRef](#)]
5. Ma, S.S.K.; Hisatomi, T.; Maeda, K.; Moriya, Y.; Domen, K. Enhanced Water Oxidation on Ta₃N₅ Photocatalysts by Modification with Alkaline Metal Salts. *J. Am. Chem. Soc.* **2012**, *134*, 19993–19996. [[CrossRef](#)]
6. Di, T.; Xu, Q.; Ho, W.; Tang, H.; Xiang, Q.; Yu, J. Review on Metal Sulphide-based Z-scheme Photocatalysts. *ChemCatChem* **2019**, *11*, 1394–1411. [[CrossRef](#)]
7. Fu, J.; Xu, Q.; Low, J.; Jiang, C.; Yu, J. Ultrathin 2D/2D WO₃/g-C₃N₄ step-scheme H₂-production photocatalyst. *Appl. Catal. B Environ.* **2019**, *243*, 556–565. [[CrossRef](#)]
8. Yuan, Y.; Shen, Z.; Wu, S.; Su, Y.; Pei, L.; Ji, Z.; Ding, M.; Bai, W.; Chen, Y.; Yu, Z.-T.; et al. Liquid exfoliation of g-C₃N₄ nanosheets to construct 2D-2D MoS₂/g-C₃N₄ photocatalyst for enhanced photocatalytic H₂ production activity. *Appl. Catal. B Environ.* **2019**, *246*, 120–128. [[CrossRef](#)]
9. Zhang, Q.; Zhang, J.; Zhang, L.; Cao, M.; Yang, F.; Dai, W.-L. Facile construction of flower-like black phosphorus nanosheet@ZnIn₂S₄ composite with highly efficient catalytic performance in hydrogen production. *Appl. Surf. Sci.* **2020**, *504*, 144366. [[CrossRef](#)]
10. Wang, W.; Ng, T.W.; Ho, W.; Huang, J.; Liang, S.; An, T.; Li, G.; Yu, J.C.; Wong, P.K. CdIn₂S₄ microsphere as an efficient visible-light-driven photocatalyst for bacterial inactivation: Synthesis, characterizations and photocatalytic inactivation mechanisms. *Appl. Catal. B Environ.* **2013**, *129*, 482–490. [[CrossRef](#)]
11. Bhirud, A.; Chaudhari, N.; Nikam, L.; Sonawane, R.; Patil, K.; Baeg, J.-O.; Kale, B. Surfactant tunable hierarchical nanostructures of CdIn₂S₄ and their photohydrogen production under solar light. *Int. J. Hydrog. Energy* **2011**, *36*, 11628–11639. [[CrossRef](#)]
12. Koelmans, H.; Grimmeiss, H. The photoconductivity of CdIn₂S₄ activated with Cu or Au. *Antivir. Res.* **1959**, *25*, 1287–1288. [[CrossRef](#)]
13. Vu, M.-H.; Nguyen, C.-C.; Sakar, M.; Do, T.-O. Ni supported CdIn₂S₄ spongy-like spheres: A noble metal free high-performance sunlight driven photocatalyst for hydrogen production. *Phys. Chem. Chem. Phys.* **2017**, *19*, 29429–29437. [[CrossRef](#)] [[PubMed](#)]
14. Fukui, M.; Omori, Y.; Kitagawa, S.-Y.; Tanaka, A.; Hashimoto, K.; Kominami, H. Visible light-induced diastereoselective semihydrogenation of alkynes to cis-alkenes over an organically modified titanium(IV) oxide photocatalyst having a metal co-catalyst. *J. Catal.* **2019**, *374*, 36–42. [[CrossRef](#)]
15. Shen, X.-Z.; Guo, J.; Liu, Z.-C.; Xie, S.-M. Visible-light-driven titania photocatalyst co-doped with nitrogen and ferrum. *Appl. Surf. Sci.* **2008**, *254*, 4726–4731. [[CrossRef](#)]
16. He, X.; Zhang, C. Recent advances in structure design for enhancing photocatalysis. *J. Mater. Sci.* **2019**, *54*, 8831–8851. [[CrossRef](#)]
17. Zhang, B.; Shi, H.; Hu, X.; Wang, Y.; Liu, E.; Fan, J. A novel S-scheme MoS₂/CdIn₂S₄ flower-like heterojunctions with enhanced photocatalytic degradation and H₂ evolution activity. *J. Phys. D Appl. Phys.* **2020**, *53*, 205101. [[CrossRef](#)]
18. Min, W.; Guo-Qiang, T.; Dan, Z.; Bin, L.; Ying, W.; Ming-Yue, D.; Hui-Jun, R.; Ao, X.; Yun, L. Synthesis and Mechanism of Direct Z-Scheme Zn₂SnO_(4-x)N_x/ZnO_(1-y)N_y Heterojunction Photocatalyst. *Chin. J. Inorg. Chem.* **2019**, *9*, 1551–1560.
19. Sun, Y.; Meng, X.; Dall’Agnese, Y.; Dall’Agnese, C.; Duan, S.; Gao, Y.; Chen, G.; Wang, X.-F. 2D MXenes as Co-catalysts in Photocatalysis: Synthetic Methods. *Nano-Micro Lett.* **2019**, *11*, 79. [[CrossRef](#)]
20. Ghosh, S.; Azad, U.P.; Singh, A.K.; Singh, A.K.; Prakash, R. Facile Synthesis of MoS_x and MoS_x-rGO Composite: Excellent Electrocatalyst for Hydrogen Evolution Reaction. *ChemistrySelect* **2017**, *2*, 11590–11598. [[CrossRef](#)]
21. Li, X.; Wang, B.; Shu, X.; Wang, N.; Xu, G.; Zhang, X.; Lv, J.; Wu, Y. An amorphous MoS_x modified g-C₃N₄ composite for efficient photocatalytic hydrogen evolution under visible light. *RSC Adv.* **2019**, *9*, 15900–15909. [[CrossRef](#)]
22. Li, X.; Tang, C.; Zheng, Q.; Shao, Y.; Li, D. Amorphous MoS_x on CdS nanorods for highly efficient photocatalytic hydrogen evolution. *J. Solid State Chem.* **2017**, *246*, 230–236. [[CrossRef](#)]
23. Tzanidis, I.; Bairamis, F.; Sygellou, L.; Andrikopoulos, K.S.; Avgeropoulos, A.; Konstantinou, I.; Tasis, D. Rapid Microwave-Assisted Synthesis of CdS/Graphene/MoS_x Tunable Heterojunctions and Their Application in Photocatalysis. *Chem. A Eur. J.* **2020**, *26*, 6643–6651. [[CrossRef](#)] [[PubMed](#)]

24. Fu, X.; Zhang, L.; Liu, L.; Li, H.; Meng, S.; Ye, X.; Chen, S. In situ photodeposition of MoS_x on CdS nanorods as a highly efficient cocatalyst for photocatalytic hydrogen production. *J. Mater. Chem. A* **2017**, *5*, 15287–15293. [[CrossRef](#)]
25. Bariki, R.; Majhi, D.; Das, K.; Behera, A.; Mishra, B.G. Facile synthesis and photocatalytic efficacy of UiO-66/CdIn₂S₄ nanocomposites with flowerlike 3D-microspheres towards aqueous phase decontamination of triclosan and H₂ evolution. *Appl. Catal. B Environ.* **2020**, *270*, 118882. [[CrossRef](#)]
26. Liu, C.; Li, X.; Li, J.; Zhou, Y.; Sun, L.; Wang, H.; Huo, P.; Ma, C.; Yan, Y. Fabricated 2D/2D CdIn₂S₄/N-rGO multi-heterostructure photocatalyst for enhanced photocatalytic activity. *Carbon* **2019**, *152*, 565–574. [[CrossRef](#)]

Publisher's Note: MDPI stays neutral with regard to jurisdictional claims in published maps and institutional affiliations.



© 2020 by the authors. Licensee MDPI, Basel, Switzerland. This article is an open access article distributed under the terms and conditions of the Creative Commons Attribution (CC BY) license (<http://creativecommons.org/licenses/by/4.0/>).